A Complete Skull from Dmanisi, Georgia, and the Evolutionary Biology of Early *Homo*

David Lordkipanidze,[1]* Marcia S. Ponce de León,[2] Ann Margvelashvili,[1,2] Yoel Rak,[3] G. Philip Rightmire,[4] Abesalom Vekua,[1] Christoph P. E. Zollikofer[2]*

The site of Dmanisi, Georgia, has yielded an impressive sample of hominid cranial and postcranial remains, documenting the presence of *Homo* outside Africa around 1.8 million years ago. Here we report on a new cranium from Dmanisi (D4500) that, together with its mandible (D2600), represents the world's first completely preserved adult hominid skull from the early Pleistocene. D4500/D2600 combines a small braincase (546 cubic centimeters) with a large prognathic face and exhibits close morphological affinities with the earliest known *Homo* fossils from Africa. The Dmanisi sample, which now comprises five crania, provides direct evidence for wide morphological variation within and among early *Homo* paleodemes. This implies the existence of a single evolving lineage of early *Homo*, with phylogeographic continuity across continents.

Excavations at Dmanisi, Georgia, have yielded hominid fossils, a rich vertebrate fauna, and Mode I (Oldowan) stone artifacts co-occurring in well-understood geological and taphonomic contexts. Occupation of the site began shortly after 1.85 million years ago (Ma) and is documented until about 1.77 Ma (*1*–*6*). The temporal and geographic setting and the preservation of at least five hominid individuals make Dmanisi a site that is crucial in understanding patterns of variation, biogeography, and evolution within emergent *Homo*. The generalized (primitive) craniomandibular morphology, small cranial capacity, moderate body size, and a mosaic of primitive and derived postcranial features link the Dmanisi sample to largely contemporaneous fossils from Africa attributed to *H. habilis* and/or *H. erectus*. Various features of the cranial vault and base also indicate affinities to *H. erectus* from East Asia (*4*, *5*, *7*, *8*).

Here we present a complete cranium (Fig. 1) that substantially expands the range of variation seen in the Dmanisi sample (Fig. 2), with implications as to the early evolutionary history of the genus *Homo*. Specimen D4500 was recovered in 2005 from the base of layer B1y in Block 2 of the Dmanisi excavation area (fig. S1) (*9*). D4500 represents the same individual as mandible D2600, found 5 years earlier (*10*). The anatomical association of D4500 and D2600 (hereafter "skull 5") constitutes the most complete adult skull known from Early Pleistocene *Homo* (hereafter "early *Homo*"; the definition of Pleistocene follows the new terminology). Skull 5 is probably associated with the postcranial elements of an adult individual with nearly modern human body proportions [(*5*); supplementary text S1 and fig. S1]. Because skull 5 is intact and free from taphonomic deformation, it is now possible to document the morphology of an entire adult cranium with its associated mandible and teeth and to study anatomy not previously known for early *Homo*.

Description of Cranium D4500

The morphology of skull 5 stands apart from that of any other known fossil *Homo* specimen through its combination of a small braincase with a large prognathic face (Fig. 1, Table 1, supplementary text S2 and S3, figs. S2 and S3, and tables S1 to S3).

Braincase

The endocranial volume, (ECV) evaluated from computed tomography (CT) data, is 546 ± 5 cm^3. Coupled with its small ECV, the braincase is low but comparatively wide and basally elongate. The frontal squama is moderately sloping. The parietals are bossed and exhibit only slight midline keeling in their posterior half. The zygomatic arches are massive, and spacious temporal fossae indicate voluminous masticatory muscles. The temporal lines are well separated from each other (minimum distance from cranial midplane 12 mm behind bregma: 20 mm). The temporal bone exhibits prominent supramastoid crests and laterally wide porial saddles, which give the neurocranium a squat, bell-like shape when viewed from the rear.

The upper squama of the occipital bone has a marked protuberance immediately below its lambdoid margin, which extends across the midplane by ~30 mm on either side. The prominence of this "lambdoid hump," together with a massive protruding inion, lends the upper occipital plane a nearly vertical orientation, whereas the nuchal plane is only moderately inclined (21°) relative to the Frankfurt horizontal (FH) plane. The occipital transverse torus is ruggedly built, and the nuchal region is deeply sculpted. A bilaminar crest linking inion with opisthion suggests a strong nuchal ligament. The mastoid processes are large and steeply inclined medially. Their inferior portion is compressed mediolaterally to form a distinctive flange-like structure that extends posteriorly. Overall, cranial superstructures of D4500 are massive and more prominent than in the other Dmanisi individuals, suggesting that it represents a male.

Temporal Bones and Cranial Base

The right zygomatic arch exhibits in vivo deformation indicating a healed but displaced multiple fracture behind the masseteric origin. The left temporomandibular joint (TMJ) as well as the left mandibular condyle bear evidence of degenerative arthritic deformation. The right TMJ and left zygomatic arch are unaffected by pathology. There is marked lateral extension of the TMJ, with 61% of the glenoid fossa beyond the external wall of the vault, below the zygomatic shelf. The fossa itself is shallow, transversely oriented (tympanomedian angle 3°), and has a low anterior wall that merges smoothly with the preglenoid planum. The tympanic plate is massive and exhibits a prominent vaginal process. Medially, the tympanic is expanded to form a robust supratubarius process. The petrous pyramid closely approaches the wall of the basioccipital, thus reducing the foramen lacerum to a crevice. The main axis of the pyramid forms an angle of 34° (petromedian angle) with the midsagittal plane. The foramen magnum is oval in shape and level (inclination 0°) with respect to the FH. Basicranial flexion, as measured by the orientation of the clival plane relative to the sphenoid plane, is low (128°).

Face

Contrasting with the small braincase, the face of skull 5 is among the largest and most prognathic known from early *Homo*. The glabellar region is massive and substantially overhangs the midface. The orbits are overarched by thick bar-like supraorbital tori; a shallow post-toral shelf (rather than a sulcus) extends posteriorly toward the frontal squama. Postorbital constriction is marked. The zygomatic processes of the maxillae are massive and laterally flaring. Their anterior surface is vertically oriented and coincides with the orbital plane, thus forming a zygomatico-orbital plane (fig. S2). As a consequence of the tall and wide midface, the zygomatico-alveolar crests are markedly angled. The roots of the zygomatic processes originate between the first and second molars. The nasal floor is delimited anteriorly by a smooth (rather than sharply angled) sill. The inclination of the naso-alveolar clivus relative to the alveolar plane is 42°. The subnasal portion of the clivus

[1]Georgian National Museum, 3 Purtseladze Street, 0105 Tbilisi, Georgia. [2]Anthropological Institute and Museum, Winterthurerstrasse 190, 8057 Zurich, Switzerland. [3]Department of Anatomy and Anthropology, Sackler Faculty of Medicine, Tel Aviv University, Tel Aviv, 69978, Israel. [4]Department of Human Evolutionary Biology, Harvard University, Cambridge, MA, USA.

*Corresponding author. E-mail: dlordkipanidze@museum.ge (D.L.); zolli@aim.uzh.ch (C.P.E.Z.)

is slightly concave, whereas its alveolar portion is convex, covering the large incisor roots. The palate is long and arched; the incisive foramen is located at the position of the second premolar (P^4), indicating marked prognathism of the maxilla and anterior dentition.

Dentition

The upper and lower dentition of skull 5 is heavily worn, and crown morphologies are only partially preserved. Estimated molar dimensions are comparatively large, and maxillary as well as mandibular molar sizes increase from M1 to M3 (Table 1 and table S3A). Judging from root orientation, the maxillary incisors were strikingly procumbent. The open bite (structural non-occlusion of the incisors), rounded labial wear surfaces on upper incisors and rounded lingual wear surfaces on lower incisors, respectively, and labiolingually oriented striations on these surfaces suggest that the anterior dentition was used in paramasticatory activities such as gripping (*11*). The first maxillary premolars (P^3s) are situated posterolaterally to Cs, such that massive C/P^3 juga square off the front of the maxilla. Similarly massive C/P_3 juga are present in the mandible D2600 (*12*). P^3s have three roots; P^4s are double-rooted, with the buccal root exhibiting two canals (three-rooted P^3s and double-rooted P^4s have also been reported for other early *Homo* specimens; see table S3B). The P_3s of mandible D2600 have two roots (the distal root with two canals) (*12*). The P_4s are not preserved.

Fig. 1. Dmanisi cranium D4500 and associated mandible D2600. (**A** and **B**) Anterior and posterior views; (**C** and **D**) superior and inferior views; (**E** and **F**) left and right views; (**G**) cranium with articulated mandible. Scale bar, 5 cm.

Comparative Analysis

Skull 5 is the first complete specimen to provide evidence of how the face (including the mandible) of adult early *Homo* was oriented and positioned relative to the braincase. Hitherto, complete craniomandibular morphology of early *Homo* was represented by two adolescents, whose facial skeletons were not yet fully developed (KNM-WT 15000 and D2700/D2735) (*2*, *13*), and the senile Dmanisi individual D3444/D3900, whose gnathic morphology was strongly modified by alveolar bone resorption after tooth loss (*3*, *4*) (Fig. 2). Among other adult early *Homo* specimens from Africa and East Asia, anatomical connections between preserved neurocranial and maxillofacial parts are typically incomplete, and facial-to-neurocranial orientation remains a matter of debate (*14*, *15*). The current perception of skull morphology of early *Homo* is thus strongly influenced by adolescent representatives (and the less complete and taphonomically distorted adult cranium KNM-ER 1813) that exhibit comparatively orthognathic faces with lightly built superstructures. The architecture of skull 5 now indicates that small-brained, large-faced, remarkably prognathic and robust morphologies all belonged to the normal range of variation of early *Homo*.

The ECV of skull 5 (546 cm^3) represents the smallest of the Dmanisi sample (skulls 1 to 4: 601 to 730 cm^3), and it is at the lower end of variation of the *H. habilis* hypodigm [509 to 687 cm^3 (*16*, *17*)]. Stature and body mass estimates obtained from the postcranial elements that are probably associated with skull 5 [146 to 166 cm, 47 to 50 kg (*5*)] place this individual within the range of variation estimated for early *Homo* and at the lower end of variation of African *H. erectus* and modern humans (*18*). The skull 5 individual thus provides the first evidence that early *Homo* comprised adult individuals with small brains but body mass, stature, and limb proportions reaching the lower range limit of modern human variation (*5*, *18*). Combining ECV and body mass data, the encephalization quotient (EQ) of the skull 5 individual is estimated as ~2.4, which is within the range of variation for *Australopithecus* (*16*). The larger ECV of early *Homo* as compared to *Australopithecus africanus* [340 to 515 cm^3 (*16*)] and *Au. sediba* [420 cm^3 (*19*)] might thus primarily reflect an evolutionary increase in body size rather than increased encephalization.

Although similarities between Dmanisi and eastern African fossils attributed to *H. ergaster* and *H. erectus* have previously been documented

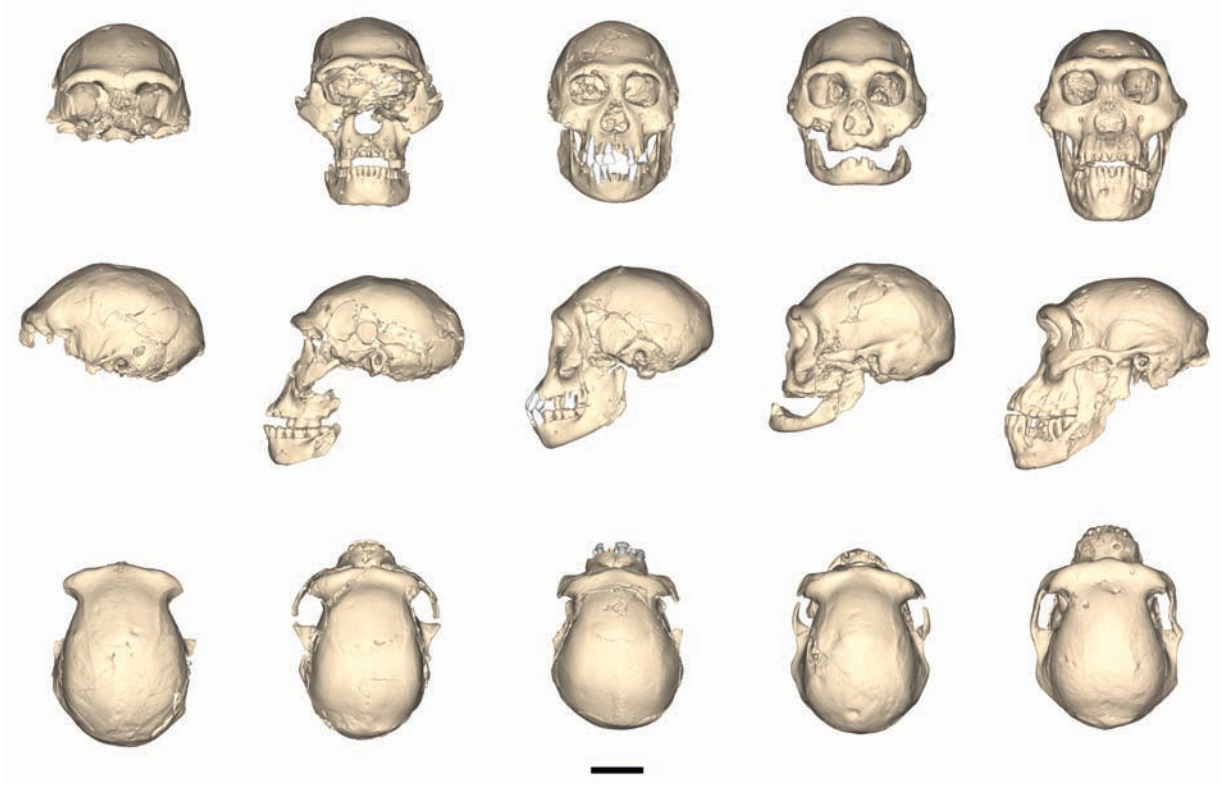

Fig. 2. The Dmanisi paleodeme. CT-based visualizations, from left to right: D2280 (skull 1), D2282/D211 (skull 2), D2700/D2735 (skull 3), D3444/D3900 (skull 4), D4500/D2600 (skull 5). Scale bar, 5 cm. See fig. S3 for a full set of standard views.

(*4*, *7*, *8*, *20*), skull 5 permits us to widen the scope of comparisons (supplementary text S4 and table S4). In midfacial architecture, skull 5 exhibits morphological affinities with the broadly contemporaneous African specimens SK 847 (fig. S4) and OH 65 (*21*), as well as with early representatives of *Homo* in eastern Africa such as KNM-ER 1470 and KNM-ER 62000, dated to ~2.0 to 1.9 Ma (*15*). In all these specimens, the naso-alveolar clivus is moderately sloping and laterally wide, curving around the buccal roots of the P^3s.

The Chemeron temporal fragment, dated to 2.4 Ma, was proposed as the earliest fossil evidence of *Homo* (*22*, *23*), but given the wide variation in TMJ position and morphology in the Dmanisi and early *Homo* samples (table S4), this assignment remains inconclusive. However, the maxilla of skull 5 is similar in overall form and dento-alveolar features to the well-preserved early *Homo* maxilla A.L. 666-1 from Hadar, Ethiopia, with a geological age of 2.33 Ma (*24*) (fig. S4 and table S4). The generic and chronological status of A.L. 666-1 has recently been questioned, and *A. sediba* (1.977 Ma) has been proposed instead as a potential ancestor of the *Homo* lineage (*25*). The close morphological affinities between A.L. 666-1, additional early *Homo* specimens from eastern Africa such as OH 65 and KNM-ER 1470 (supplementary text S4), and now skull 5, however, effectively falsify such a scenario (*26*).

Table 1. Craniodental dimensions of skull 5. Linear dimensions are in millimeters, angles in degrees, areas in square millimeters, and volumes in cubic centimeters.

Endocranial volume	546 (541–551)
Glabella-opisthocranion length	165
Basion-bregma height	92
Nasion-bregma length	86
Biporionic breadth	123
Maximum parietal breadth	109
Cranial base angle (CBA4)	128
Minimum frontal breadth	75
Supraorbital torus thickness	12
Upper facial width (bi-frontomalare temporale)	112
Biorbital width (bi-frontomalare orbitale)	99
Bizygomatic width	149
Midfacial width (bi-zygomaxillare)	109
Nasion-prosthion length	73
Nasion-basion length	99
Basion-prosthion length	127
Palate length (orale-staphylion)	75
Palate width (at M2)	35
Naso-alveolar clivus angle	42
Symphyseal height	50
Molar crown area (buccolingual width x mesiodistal width) M^1, M^2, M^3	159, 197, 208
Molar crown area (buccolingual width x mesiodistal width) M_1, M_2, M_3	160, 186, 217

Variation now established by the enlarged Dmanisi sample is crucial to identifying patterns of variation among and between paleospecies of early *Homo*. Several studies provide evidence for variation along and across a single evolving lineage of early *Homo* (*27*, *28*), with differences between fossil specimens primarily reflecting intraspecific variation at the population level and

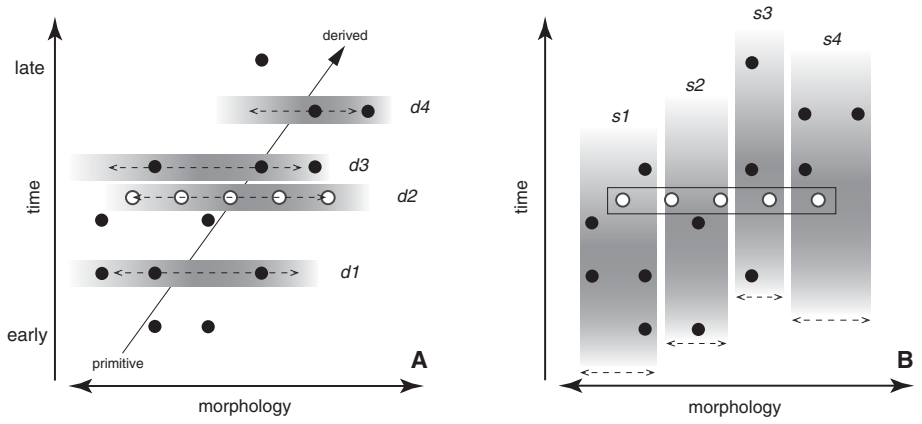

Fig. 3. Two contrasting hypotheses about the evolution of early *Homo*. Hypothesis (**A**) posits that the fossil record samples paleodemes (horizontal bands, *d1* to *d4*) of a phyletically evolving early *Homo* lineage, each with a separate geographic focus but overlapping in time and morphology. Selection and drift result in an overall morphocline from early generalized to late derived forms (diagonal arrow). This hypothesis is compatible with a wide range of variation within paleodemes of a lineage (dashed double arrows) and is most compatible with the evidence of morphological variation in the Dmanisi deme (white dots). Hypothesis (**B**) posits that the fossil record [same dots as in (A)] samples distinct paleospecies (vertical bands, *s1* to *s4*) overlapping in time and space. This hypothesis predicts that morphological variation within each lineage is restricted (dashed double arrows), which is incompatible with the combined evidence of multiple contemporary but morphologically disparate crania from Dmanisi (white dots).

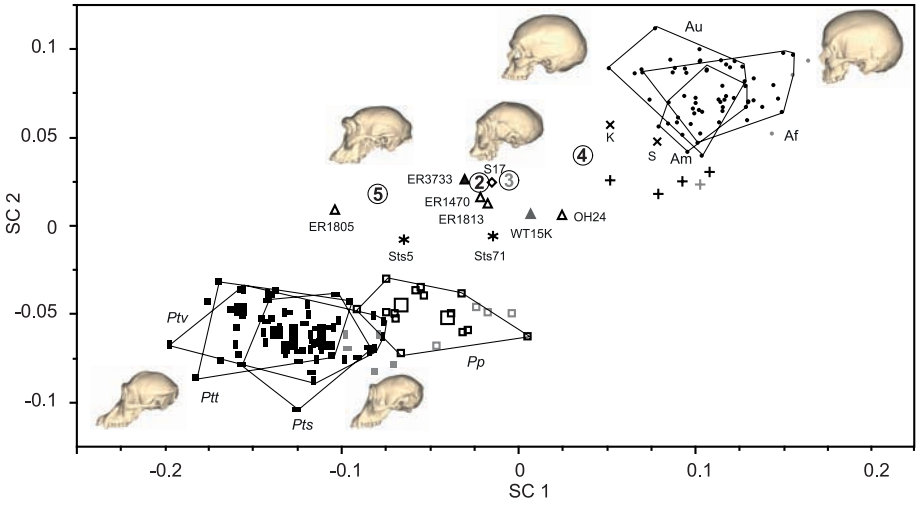

Fig. 4. Shape variation of the Dmanisi crania in comparative context. Dmanisi crania [2:D2282 (skull 2), 3:D2700 (skull 3 and picture), 4:D3444 (skull 4), 5: D4500 (skull 5 and picture)]; African early *Homo* (triangles with specimen names); *A. africanus* (asterisks); *H. erectus*]ava (diamond); Kabwe and Steinheim (crosses); *H. neanderthalensis* (plus signs); *H. sapiens* (dots and pictures; populations from Africa, Australia, and America); *P. troglodytes*: *P. t. troglodytes* (solid squares and pictures), *P. t. verus* (vertical rectangles), *P. t. schweinfurthii* (horizontal rectangles); *P. paniscus* (open squares). Black symbols indicate adult individuals; gray symbols indicate subadult individuals. Large symbols indicate male and female averages. Shape component SC1 captures within-group cranial variation from large-faced/prognathic to small-faced/orthognathic individuals; SC2 captures shape change associated with grade shifts in neurocranial size between taxa.

evolutionary change within a species over time (Fig. 3A). Other studies, however, interpret variation in small samples of early African *Homo* as reflecting taxonomic species diversity (*15*, *29*–*31*) and posit three or more largely contemporary paleospecies (*H. rudolfensis, H. habilis*, and *H. erectus*). According to this interpretation (Fig. 3B), morphological differences among individual fossil specimens indicate interspecific differences and concomitant phyletic diversification.

Testing these contrasting hypotheses depends on information about variation within paleodemes; that is, within populations of a fossil species at a given point in space and time (*32*) (Fig. 3). A fossil sample is likely to represent a paleodeme if two conditions are met. It must come from a spatially and temporally constrained stratigraphic and taphonomic setting [which is the case for Dmanisi (*4*, *5*)], and within-sample variation must be similar in range and mode to within-deme variation in closely related extant species.

Geometric morphometric analysis and resampling statistics show that craniomandibular shape variation among the Dmanisi hominids is congruent with patterns and ranges of variation in chimpanzee and bonobo demes (*Pan troglodytes troglodytes*, *P. t. verus*, *P. t. schweinfurthii*, and *P. paniscus*) and in a global sample of *H. sapiens* (Fig. 4, supplementary text S5 to S7, and figs. S7 to S9). Within all groups, variation in cranial shape is mainly due to interindividual differences in size and orientation of the face relative to the braincase. The Dmanisi sample, including skull 5, thus represents normal within-deme variation, ranging from small-faced relatively orthognathic (typically female and/or subadult) individuals to large-faced relatively prognathic (typically male) individuals.

Comparative analysis of nonmetric cranial characters also indicates that within-deme variation is substantial and wider than typically recognized (supplementary text S2 to S4 and table S4). The Dmanisi paleodeme shows variation in maxillofacial features, which have been interpreted as evidence for taxonomic diversity in eastern African fossils (*15*, *31*).

The Dmanisi sample thus represents the best currently available example of cranial form and form variation within the early *Homo* lineage. It can tentatively be characterized as follows (figs. S2 and S3): face with flaring, vertically oriented zygomatic processes that are coplanar with the orbital plane; similar upper and midfacial widths; markedly angled zygomaticoalveolar crests; marked alveolar prognathism; C roots exhibiting parallel orientation relative to the cranial midplane; naso-alveolar clivus moderately sloping and laterally delimited by C and/or P^3 juga; and ECV greater than ~500 cm^3. These features also discriminate early *Homo* from nonrobust *Australopithecus* species, which exhibit a more protruding but less sloping naso-alveolar clivus; inclined maxillary zygomatic processes; moderately curved zygomaticoalveolar crests; and superomedially tapering canine juga, which laterally delimit the anterior surface of the maxilla. Other features of early *Homo*, such as three-rooted premolars, marked postorbital narrowing, a shallow glenoid fossa, and a moderate degree of basicranial flexion, represent pleisomorphic (primitive) character states variably shared with the *Australopithecus* species.

Discussion

As already noted by Darwin, recognizing species diversity comes "at the expense of admitting much variation" within species [(*33*), p. 51]. Together with data from *Au. afarensis* paleodemes such as A.L. 333 (*34*–*36*), Dmanisi adds to the growing evidence that intrademic and intraspecific

variation in Plio-Pleistocene fossil hominids tends to be misinterpreted as species diversity, especially when single fossil specimens from different localities are compared with each other (*37*). Evidence from skull 5 and the other four Dmanisi specimens indicates that cranial shape variation within early *Homo* paleodemes was similar in mode and range to that seen within modern *Pan* demes. Furthermore, Dmanisi indicates that an important proportion of character state variation in nonmetric features reflects intrademic variation rather than real species diversity. These findings have several implications for the interpretation of morphological diversity in the fossil record of early *Homo*.

When seen from the Dmanisi perspective, morphological diversity in the African fossil *Homo* record around 1.8 Ma probably reflects variation between demes of a single evolving lineage, which is appropriately named *H. erectus*. The hypothesis of multiple independent lineages (paleospecies) (*15*, *31*) appears less parsimonious, especially in the absence of empirical evidence for adaptation to separate ecological niches. The hypothesis of phyletic evolution within a single but polymorphic lineage raises a classificatory but not evolutionary dilemma, and it is premature to describe the rate(s) of evolution in this lineage, given the small available samples. Specimens previously attributed to *H. ergaster* are thus sensibly classified as a chronosubspecies, *H. erectus ergaster*. The Dmanisi population probably originated from an Early Pleistocene expansion of the *H. erectus* lineage from Africa, so it is sensibly placed within *H. e. ergaster* and formally designated as *H. e. e. georgicus* to denote the geographic location of this deme [thus retracting the species status given earlier to mandible D2600 (*12*)].

Given the scattered and fragmentary fossil record in Africa that predates Dmanisi, questions of earliest African *Homo* phylogenetics and classification remain unresolved. It remains to be tested whether all of the fossils currently allocated to the taxa *H. habilis* and *H. rudolfensis* belong to a single evolving *Homo* lineage. Although we regard this null hypothesis as parsimonious and fully compatible with new evidence from Dmanisi, alternative scenarios exist. Given the range of variation seen in the Dmanisi paleodeme, there is no convincing signature, at present, of early *Homo* cladogenesis. The African fossils that postdate the Dmanisi ensemble show brain size increase and correlated change in craniofacial morphology within the evolving lineage of *H. erectus*. Moreover, it is likely that both the underpinning of the East Asian dispersal of *H. erectus*, as well as the roots of subsequent *H. erectus* evolution in Africa (for example, OH 9, Daka), shared greater craniofacial robusticity.

The new evidence from the ancient Dmanisi deme of early *Homo* reinforces the strong African affinities previously recognized for this early Eurasian outpost of our genus (*7*). Variation between continents may thus provide insight into the evolutionary population dynamics of early *Homo*. It is well known from the upper Pleistocene dispersal of modern humans from Africa that genetic and phenetic variation within demes decreases with geographic distance from Africa, due to serial founder effects and population bottlenecks. For example, modern human phenetic variation in western and eastern Asia is 95 and 85% of African variation, respectively (*38*). The expansion of early *Homo* from Africa might have occurred at longer time scales, so direct comparisons must remain tentative. Nevertheless, the observation that Dmanisi conserves a substantial proportion of cranial shape and its variation among early African *Homo* speaks for genetic continuity between Africa and Eurasia. Because intrademic variation at Dmanisi is similar to that found in extant and extinct near relatives, the effective population size of early *Homo* in western Asia might have been similar [N_e > 10,000 (*39*)]. Furthermore, the remarkably large and robust dentognathic remains of early *H. erectus* from Java (Trinil/Sangiran) (*40*, *41*) exhibit close affinities with skull 5 (tables S2 to S4). This provides evidence for morphological (and presumably underpinning genetic) continuity across large geographic distances, and for the preservation in East Asia of an appreciable proportion of the variation originally present within paleodemes of early *Homo* in Africa (*20*, *42*–*44*) (fig. S8).

Contrasting with early *Homo* population continuity across continents, current paleontological data indicate a low degree of similarity between contemporaneous mammalian genera in Africa and at Dmanisi (*5*), implying a generally low rate of faunal exchange between Africa and Asia before and around 1.8 Ma (*45*). As suggested earlier (*46*), the populational, ecological, and evolutionary dynamics of early *Homo* probably differed significantly from those of coeval large mammals, including other hominid lineages. Theoretical considerations indicate that the long-range dispersal rate of a population mainly depends on rates of reproduction and local habitat expansion (*47*) and that intragroup cooperation can play an important role in population persistence (*48*). Various features such as derived lower limb and foot morphologies (*5*, *49*), tool-mediated widening of the dietary niche toward meat eating (*4*, *6*), and increased levels of intragroup cooperation (*3*) might have led to increased rates of reproduction, survival, and mobility in early *Homo* and the consequent establishment of stable populations outside Africa. Skull 5 and the other members of the Dmanisi paleodeme now indicate that early *Homo* expanded from Africa to ultimately establish substantial populations in western Asia. This earliest hominid dispersal pre-dated any significant increase in brain size. Further analyses are required to test and modify the attendant hypotheses. Ultimately, identifying hominid paleodemes and assessing within-deme variation (*32*) will be key to understanding mechanisms of evolution and geographic dispersal of early *Homo*.

References and Notes

1. L. Gabunia *et al.*, *Science* **288**, 1019–1025 (2000).
2. A. Vekua *et al.*, *Science* **297**, 85–89 (2002).
3. D. Lordkipanidze *et al.*, *Nature* **434**, 717–718 (2005).
4. D. Lordkipanidze *et al.*, *Anat. Rec. A Discov. Mol. Cell Evol. Biol.* **288A**, 1146–1157 (2006).
5. D. Lordkipanidze *et al.*, *Nature* **449**, 305–310 (2007).
6. R. Ferring *et al.*, *Proc. Natl. Acad. Sci. U.S.A.* **108**, 10432–10436 (2011).
7. G. P. Rightmire, D. Lordkipanidze, A. Vekua, *J. Hum. Evol.* **50**, 115–141 (2006).
8. G. P. Rightmire, D. Lordkipanidze, in *Out of Africa I. The First Hominin Colonization of Eurasia,* J. G. Fleagle, J. J. Shea, F. E. Grine, A. L. Baden, R. E. Leakey, Eds. (Springer, New York, 2010), pp. 225–243.
9. Supplementary materials are available on *Science* Online.
10. L. Gabunia, M. A. de Lumley, A. Vekua, D. Lordkipanidze, *Archaeol. Ethnol. Anthropol. Eurasia* **4**, 145 (2002).
11. M. Lozano, J. M. Bermúdez de Castro, E. Carbonell, J. L. Arsuaga, *J. Hum. Evol.* **55**, 713–728 (2008).
12. L. Gabounia, M. A. de Lumley, A. Vekua, D. Lordkipanidze, H. de Lumley, *C. R. Palevol.* **1**, 243–253 (2002).
13. A. Walker, R. Leakey, Eds., *The Nariokotome* Homo erectus *Skeleton* (Springer, Berlin, 1993).
14. T. G. Bromage *et al.*, *J. Clin. Pediatr. Dent.* **33**, 43–54 (2008).
15. M. G. Leakey *et al.*, *Nature* **488**, 201–204 (2012).
16. R. L. Holloway, D. Broadfield, M. Yuan, *Brain Endocasts - The Paleoneurological Evidence*, G. T. Schwartz, I. Tattersall, Eds., vol. 3 of *The Human Fossil Record* (Wiley, Hoboken, NJ, 2004).
17. G. P. Rightmire, *Am. J. Phys. Anthropol.* **124**, 109–123 (2004).
18. T. W. Holliday, *Curr. Anthropol.* **53** (S6), S330–S345 (2012).
19. K. J. Carlson *et al.*, *Science* **333**, 1402–1407 (2011).
20. K. L. Baab, *J. Hum. Evol.* **54**, 827–847 (2008).
21. R. J. Blumenschine *et al.*, *Science* **299**, 1217–1221 (2003).
22. A. Hill, S. Ward, A. Deino, G. Curtis, R. Drake, *Nature* **355**, 719–722 (1992).
23. R. J. Sherwood, S. C. Ward, A. Hill, *J. Hum. Evol.* **42**, 153–184 (2002).
24. W. H. Kimbel, D. C. Johanson, Y. Rak, *Am. J. Phys. Anthropol.* **103**, 235–262 (1997).
25. R. Pickering *et al.*, *Science* **333**, 1421–1423 (2011).
26. W. H. Kimbel, *Nature* **497**, 573–574 (2013).
27. B. Asfaw *et al.*, *Nature* **416**, 317–320 (2002).
28. G. Suwa *et al.*, *Anthropol. Sci.* **115**, 133–151 (2007).
29. B. Wood, *Koobi Fora Research Project: Hominid Cranial Remains* (Oxford Univ. Press, New York, 1991).
30. B. Wood, *Nature* **355**, 783–790 (1992).
31. F. Spoor *et al.*, *Nature* **448**, 688–691 (2007).
32. F. C. Howell, *J. Anthropol. Res.* **55**, 191 (1999).
33. C. R. Darwin, *On the Origin of Species by Means of Natural Selection, or the Preservation of Favoured Races in the Struggle for Life* (John Murray, London, ed. 5, 1869).
34. T. D. White, D. C. Johanson, in *Hominidae,* G. Giacobini, Ed. (Jaka, Milan, Italy, 1989), pp. 97–101.
35. P. L. Reno, R. S. Meindl, M. A. McCollum, C. O. Lovejoy, *Proc. Natl. Acad. Sci. U.S.A.* **100**, 9404–9409 (2003).
36. A. K. Behrensmeyer, in *The Geology of Early Humans in the Horn of Africa,* J. Quade, J. G. Wynn, Eds. (Geological Society of America Special Paper 446, 2008), pp. 203–214.
37. W. H. Gilbert, T. D. White, B. Asfaw, *J. Hum. Evol.* **45**, 255–259 (2003).
38. A. Manica, W. Amos, F. Balloux, T. Hanihara, *Nature* **448**, 346–348 (2007).
39. T. Marques-Bonet, O. A. Ryder, E. E. Eichler, *Annu. Rev. Genomics Hum. Genet.* **10**, 355–386 (2009).
40. Y. Kaifu *et al.*, *Am. J. Phys. Anthropol.* **128**, 709–726 (2005).
41. Y. Kaifu, E. Indriati, F. Aziz, I. Kurniawan, H. Baba, in *Asian Paleoanthropology: From Africa to China and Beyond*, C. Norton, D. Braun, Eds. (Springer, Dordrecht, Netherlands, 2010), pp. 143–157.
42. Y. Kaifu, F. Aziz, H. Baba, *Am. J. Phys. Anthropol.* **128**, 497–519 (2005).
43. Y. Kaifu *et al.*, *J. Hum. Evol.* **55**, 551–580 (2008).

44. C. E. Terhune, W. H. Kimbel, C. A. Lockwood, *J. Hum. Evol.* **53**, 41–60 (2007).
45. J. Agustí, D. Lordkipanidze, *Quat. Sci. Rev.* **30**, 1338–1342 (2011).
46. S. C. Antón, C. C. Swisher III, *Annu. Rev. Anthropol.* **33**, 271–296 (2004).
47. A. Hastings, *Biol. Conserv.* **78**, 143–148 (1996).
48. M. J. Hamilton *et al.*, *Proc. Natl. Acad. Sci. U.S.A.* **106**, 12255–12260 (2009).
49. H. Pontzer *et al.*, *J. Hum. Evol.* **58**, 492–504 (2010).

Acknowledgments: This research was supported by the Rustaveli Georgian National Science Foundation, the Swiss National Science Foundation, the U.S. National Science Foundation, the National Geographic Society, the L.S.B. Leakey Foundation, the American Philosophical Society, the American School for Prehistoric Research, a Rolex Award for Enterprise, BP Georgia, the Fundación Duques de Soria, the A.H. Schultz Foundation, and the Foundation for Scientific Research (University of Zurich). We thank the Dmanisi excavation team for excellent work; special thanks go to G. Kiladze. G. Nioradze was the first *H. sapiens* to encounter D4500. We gratefully acknowledge the work of the late G. Bumbiashvili, who photographed skull 5 and the other Dmanisi hominids. We thank G. Nemsadze (N. Kipshidze Central Clinical Hospital of Tbilisi State Medical University) and I. Tatishvili (A. Gvamichava Oncology National Center, Tbilisi) for CT data acquisition. We also thank the reviewers for their valuable comments, which helped to improve the manuscript. Dmanisi skull 5 is deposited at the Georgian National Museum, Tbilisi, Georgia.

Supplementary Materials
www.sciencemag.org/content/342/6156/326/suppl/DC1
Supplementary Text S1 to S6
Figs. S1 to S9
Tables S1 to S7
References (*50*–*96*)

29 March 2013; accepted 11 September 2013
10.1126/science.1238484

Stellar Spin-Orbit Misalignment in a Multiplanet System

Daniel Huber,[1]* Joshua A. Carter,[2] Mauro Barbieri,[3] Andrea Miglio,[4,5] Katherine M. Deck,[6] Daniel C. Fabrycky,[7] Benjamin T. Montet,[8] Lars A. Buchhave,[9,10] William J. Chaplin,[4,5] Saskia Hekker,[11,12] Josefina Montalbán,[13] Roberto Sanchis-Ojeda,[6] Sarbani Basu,[14] Timothy R. Bedding,[5,15] Tiago L. Campante,[4,5] Jørgen Christensen-Dalsgaard,[5] Yvonne P. Elsworth,[4,5] Dennis Stello,[5,15] Torben Arentoft,[5] Eric B. Ford,[16,17] Ronald L. Gilliland,[16] Rasmus Handberg,[4,5] Andrew W. Howard,[18] Howard Isaacson,[19] John Asher Johnson,[8] Christoffer Karoff,[5] Steven D. Kawaler,[20] Hans Kjeldsen,[5] David W. Latham,[2] Mikkel N. Lund,[5] Mia Lundkvist,[5] Geoffrey W. Marcy,[19] Travis S. Metcalfe,[5,21] Victor Silva Aguirre,[5] Joshua N. Winn[6]

Stars hosting hot Jupiters are often observed to have high obliquities, whereas stars with multiple coplanar planets have been seen to have low obliquities. This has been interpreted as evidence that hot-Jupiter formation is linked to dynamical disruption, as opposed to planet migration through a protoplanetary disk. We used asteroseismology to measure a large obliquity for Kepler-56, a red giant star hosting two transiting coplanar planets. These observations show that spin-orbit misalignments are not confined to hot-Jupiter systems. Misalignments in a broader class of systems had been predicted as a consequence of torques from wide-orbiting companions, and indeed radial velocity measurements revealed a third companion in a wide orbit in the Kepler-56 system.

The Kepler space telescope detects exoplanets by measuring periodic dimmings of light as a planet passes in front of its host star (*1*). The majority of the ~150,000 targets observed by Kepler are unevolved stars near the main sequence, because those stars provide the best prospect for detecting habitable planets similar to Earth (*2*). In contrast, the temperature and surface gravity of Kepler-56 (KIC6448890) indicate that it is an evolved star with exhausted hydrogen in its core and that it started burning hydrogen in a shell surrounding an inert helium core. Stellar evolutionary theory predicts that our Sun will evolve into a low-luminosity red giant similar in size to Kepler-56 in roughly 7 billion years.

The Kepler planet search pipeline detected two planet candidates orbiting Kepler-56 (designated as KOI-1241) (*3*) with periods of 10.50 and 21.41 days, a nearly 2:1 commensurability. The observation of transit time variations caused by gravitational interactions showed that the two candidates represent objects orbiting the same star, and modeling of these variations led to upper limits on their masses that place them firmly in the planetary regime (*4*). Kepler-56 is the most evolved star observed by Kepler with more than one detected planet. Transit observations lead to measurements of planet properties relative to stellar properties, and hence accurate knowledge of the host star is required to characterize the system. Asteroseismology enables inference of stellar properties through the measurement of oscillations excited by near-surface convection (*5*). The power spectrum of the Kepler-56 data after removing the planetary transits shows a regular series of peaks (Fig. 1), which are characteristic of stellar oscillations. By combining the measured oscillation frequencies with the effective temperature and chemical composition obtained from spectroscopy, we were able to precisely determine the properties of the host star (*6*). Kepler-56 is more than four times as large as the Sun and its mass is 30% greater (Table 1).

Nonradial oscillations in evolved stars are mixed modes, behaving like pressure modes in the envelope and like gravity modes in the core (*7*, *8*). Unlike pressure-dominated mixed modes, gravity-dominated mixed modes have frequencies that are shifted from the regular asymptotic spacing. Mixed modes are also approximately equally spaced in period (*9*). We measured the average period spacing between dipole ($l = 1$) modes in Kepler-56 to be 50 s, consistent with a first-ascent red giant (*10*).

Individual mixed dipole modes are further split into multiplets as a result of stellar rotation. Because the modes in each multiplet are on average expected to be excited to very nearly equal amplitudes, the observed relative amplitudes depend only on viewing angle relative to the stellar rotation axis (*11*). For Kepler-56, several mixed dipole modes show triplets (Fig. 1). A rotation axis perpendicular to the line of sight (inclination $i = 90°$) would have produced a frequency doublet, whereas a star viewed pole-on ($i = 0°$) would have produced no visible splitting (*6*). Therefore, the observed triplets are a clear signature of an intermediate inclination of the stellar rotation axis with respect to the line of sight. This also implies an intermediate inclination with respect to the planetary

[1]NASA Ames Research Center, MS 244-30, Moffett Field, CA 94035, USA. [2]Harvard-Smithsonian Center for Astrophysics, 60 Garden Street, Cambridge, MA 02138, USA. [3]CISAS, University of Padua, via Venezia 15, 35131 Padova, Italy. [4]School of Physics and Astronomy, University of Birmingham, Birmingham B15 2TT, UK. [5]Stellar Astrophysics Centre, Department of Physics and Astronomy, Aarhus University, Ny Munkegade 120, 8000 Aarhus C, Denmark. [6]Department of Physics, Massachusetts Institute of Technology, Cambridge, MA 02139, USA. [7]Department of Astronomy and Astrophysics, University of Chicago, Chicago, IL 60637, USA. [8]Department of Astrophysics, California Institute of Technology, Pasadena, CA 91125, USA. [9]Niels Bohr Institute, University of Copenhagen, DK-2100 Copenhagen, Denmark. [10]Centre for Star and Planet Formation, Natural History Museum of Denmark, University of Copenhagen, DK-1350 Copenhagen, Denmark. [11]Astronomical Institute "Anton Pannekoek," University of Amsterdam, 1098 XH Amsterdam, Netherlands. [12]Max-Planck-Institut für Sonnensystemforschung, 37191 Katlenburg-Lindau, Germany. [13]Institut d'Astrophysique et de Géophysique de l'Université de Liège, B 4000 Liège, Belgium. [14]Department of Astronomy, Yale University, P.O. Box 208101, New Haven, CT 06520, USA. [15]Sydney Institute for Astronomy, School of Physics, University of Sydney, Sydney, NSW 2006, Australia. [16]Center for Exoplanets and Habitable Worlds, Pennsylvania State University, University Park, PA 16802, USA. [17]Astronomy Department, University of Florida, Gainesville, FL 32111, USA. [18]Institute for Astronomy, University of Hawaii, Honolulu, HI 96822, USA. [19]Department of Astronomy, University of California, Berkeley, CA 94720, USA. [20]Department of Physics and Astronomy, Iowa State University, Ames, IA 50011, USA. [21]Space Science Institute, Boulder, CO 80301, USA.

*Corresponding author. E-mail: daniel.huber@nasa.gov